Pergamon

Geochimica et Cosmochimica Acta, Vol. 59, No. 19, pp. 3987–3995, 1995

0016-7037/95 $9.50 + .00

0016-7037(95)00261-8

Assessment of the uncertainties and limitations of quantitative elemental analysis of individual fluid inclusions using synchrotron X-ray fluorescence (SXRF)*

J. A. MAVROGENES,[1,†] R. J. BODNAR,[1] A. J. ANDERSON,[2] S. BAJT,[3] S. R. SUTTON,[3] and M. L. RIVERS[3]

[1]Fluids Research Laboratory, Department of Geological Sciences, Virginia Polytechnic Institute and State University, Blacksburg, VA 24061, USA
[2]Geology Department, St Francis Xavier University, Antigonish, Nova Scotia B2G 1CO, Canada
[3]Department of Geophysical Sciences, University of Chicago, Chicago, IL 60637, USA

(*Received October* 4, 1994; *accepted in revised form June* 4, 1995)

Abstract—Synchrotron X-ray Fluorescence (SXRF) analysis is a nondestructive analytical technique that provides compositional information from single fluid inclusions. A protocol for conducting quantitative analyses of metal concentrations in individual fluid inclusions has been developed. This has led to an understanding of the accuracy, precision, and detection limits of this technique, as well as the optimal shapes, sizes, and geometries required for reliable fluid inclusion analysis.

Aqueous fluid inclusions containing known concentrations of $SrCl_2$ were synthesized for the development and the standardization of this technique. Strontium chloride was selected because it is highly soluble, its freezing-point depression is well known (allowing us to confirm the inclusion composition using microthermometric analyses), and the energetic Sr X-rays are only mildly attenuated by quartz. To confirm the composition of the synthetic standards, solutions were measured before and after each hydrothermal run using Atomic Absorption Spectroscopy (AAS), and the freezing-point depression for each fluid inclusion was measured.

SXRF analyses were performed on beam line X26A of the National Synchrotron Light Source (NSLS) at Brookhaven National Laboratory using an 8 × 12 μm white X-ray beam. The analytical volume was calculated based on known beam dimensions and fluid inclusion geometry determined using a modified spindle stage. Elemental concentrations were determined by ratioing the Sr counts from an inclusion to the counts obtained from capillaries of known diameter containing similar solutions.

Numerous inclusions from five samples, each with a different Sr concentration, were analyzed. Within a single population the mean is very close to the known concentration, but the precision is poor, with standard deviations (1σ) from 10–39% of the mean. Errors in determining the inclusion geometry are the main contributor to the poor precision. The poor precision requires that numerous inclusions within one population be analyzed and averaged to accurately estimate the metal concentration for that population. Selection of flat-lying, equant, regularly-shaped inclusions for analysis minimizes errors resulting from inclusion geometry if quantitative results are sought. The detection limit for Sr in synthetic fluid inclusions (typically 4–15 μm thick, and 5–100 μm below the upper polished surface) is approximately 2,000 ppm Sr.

1. INTRODUCTION

In studies of hydrothermal ore deposits, one of the most often asked questions concerns the source(s) and concentrations of metals in ore-forming fluids. Theoretical calculations (Helgeson, 1992), results of experimental studies (Barnes, 1979; Keppler and Wyllie, 1991), as well as analyses of fluids from active geothermal systems (Weissberg et al., 1979), volcanoes (Symonds, 1992), and oil-field brines (Carpenter et al., 1974) provide indirect answers to these questions. The most direct and convincing evidence, however, comes from the identification and analysis of fluid inclusions associated with mineralization to determine the type and concentration of contained metals.

Numerous techniques, including electron microscopy of opened (Haynes et al., 1988) and unopened fluid inclusions (e.g., Maaskant, 1986), laser ablation-ICP (see Shepherd et al., 1985), proton-induced X-ray emission (PIXE), and gamma-ray emission (PIGE) spectroscopies (Horn and Traxel, 1987; Anderson et al., 1989; Heinrich et al., 1992) have been applied to determine metal contents of individual fluid inclusions. Furthermore, various other techniques have been used for bulk fluid inclusion analysis (reviewed by Roedder, 1990). Although data provided by these and similar studies have offered valuable insights into hydrothermal fluid chemistry, each of these techniques has limitations. Thus, results from bulk extraction techniques, in particular, are difficult to interpret because these analyses often represent a mixture of fluid inclusion generations. Recently, synchrotron X-ray fluorescence (SXRF) has been shown to be a promising technique for in situ, nondestructive qualitative to semiquantitative analysis of individual natural (Rankin et al., 1992) and synthetic (Frantz et al., 1988; Vanko et al., 1993) fluid inclusions. A general description of synchrotron radiation applications in the earth sciences is provided by Bassett and Brown (1990), and a detailed review of SXRF techniques is provided by Rivers et al. (1991).

The purpose of this study was to develop and rigorously test the SXRF technique for quantitative analysis of individual

* Presented at the fifth biennial Pan-American Conference on Research on Fluid Inclusions (PACROFI V) held May 19–21, 1994, at the Instituto de Investigaciones Electricas in Cuernavaca, Morelos, Mexico.

† *Present address:* Research School of Earth Sciences, Australian National University, Canberra, ACT 0200, Australia.

fluid inclusions. Previous attempts to use SXRF for fluid inclusion analyses have used theoretical models which assume an ideal analytical geometry to interpret spectra and calculate metal contents. However, these models were not tested by analyzing fluid inclusions of known concentration and variable (nonideal) geometry. In this study synthetic fluid inclusions of known $SrCl_2$ concentration were prepared and analyzed. The geometry of each inclusion analyzed was determined, and the calculated Sr concentration was compared to the actual (known) concentration. Those factors which most affect accurate quantitative analysis with SXRF are described.

2. EXPERIMENTAL DESIGN

The intensity of the XRF spectrum for a given element in a natural sample is a function of (1) the analytical volume being excited by the beam, (2) the concentration of the element in the analytical volume and, (3) interferences from the host phase or from phases not contained within the analytical volume. In the case of fluid inclusions in quartz, the analytical volume is that volume of fluid in the inclusion through which the beam passes. Similarly, interferences are provided by phases other than the fluid phase contained either in the inclusion or in the quartz host, and by the host quartz itself.

In order to evaluate the relative importance of each of these factors in quantitative analysis of fluid inclusions, aqueous solutions containing known concentrations of various metals were placed into silica-glass capillaries of known wall thickness and inner diameter (permitting accurate determination of analytical volume) and analyzed with SXRF. Results obtained from capillaries were used as standards for interpreting spectra obtained from inclusions of known geometry and analytical volume, but unknown concentration.

Fluid inclusions selected for SXRF analysis were photographed before the analysis so that specific fluid inclusions could be located afterwards, either to conduct duplicate analyses or to measure the inclusion geometry. A modified spindle stage (as described by Anderson and Bodnar, 1993) was used to determine the depth (d, Fig. 1) and thickness of each inclusion selected for analysis.

Synchrotron X-ray fluorescence analyses were performed on beam line X26A at the National Synchrotron Light Source, Brookhaven National Laboratory, Upton, New York. At the start of every session the analytical set-up was optimized by maximizing elemental ratios on a standard polished section of anorthite ($CaAl_2Si_2O_8$). The beam focus and position were established using a polished fluorescent material (CsI). The beam size was measured by scanning across a sharp-edged Au grid in the X and Y directions. The beam width is defined, by convention, as equal to the distance between 20% and 80% of the Au peak height. In the X direction (normal to the beam) the beam width is simply that distance, but in the Y direction the beam width is taken as the distance between 20% and 80% of the Au peak height divided by $\sqrt{2}$ because the beam crosses the sample at 45°. For all of the analyses presented here, the beam measured approximately 8 μm by 12 μm.

A doubly polished quartz chip, 100–300 μm thick, containing preselected fluid inclusions, was mounted on a pure silica glass disk and placed in a vertical, motorized X-Y-Z stage in the X-ray hutch. An optical microscope with a video camera positioned at 90° to the sample surface allowed direct observation of the sample during analysis (Fig. 1). Samples were excited by a white light (continuum energy spectrum) beam covering the range 3–30 keV, with maximum energy near 8 keV, thus only the high energy end of this spectrum excites Sr (Sr Kα critical excitation energy is 16.1 keV). X-ray spectra were collected, in air, using a Si(Li) energy dispersive detector positioned at 90° to the beam (Fig. 1). One and two dimensional scans were made by mechanically moving the sample stage in the X (horizontal) and/or Y (vertical) directions.

The incoming beam penetrates the sample at 45° to the polished surface, and the detector is also positioned at 45° to the sample. Therefore, the path length through quartz (before reaching the inclusion) for the incoming beam (Pi, Fig. 1) is equal to the path length through quartz for the outgoing X-rays (Po, Fig. 1) generated from the inclusion. From the inclusion depth this path length is easily determined since path length = depth/sin 45°, or depth/0.707. Similarly, the path length through the inclusion (stippled beam path, Fig. 1) is equal to the inclusion thickness/0.707, or can be measured directly by rotating the sample 45° (on an axis perpendicular to the beam direction) and measuring the thickness of the inclusion at the point where the beam passed through it (Fig. 1).

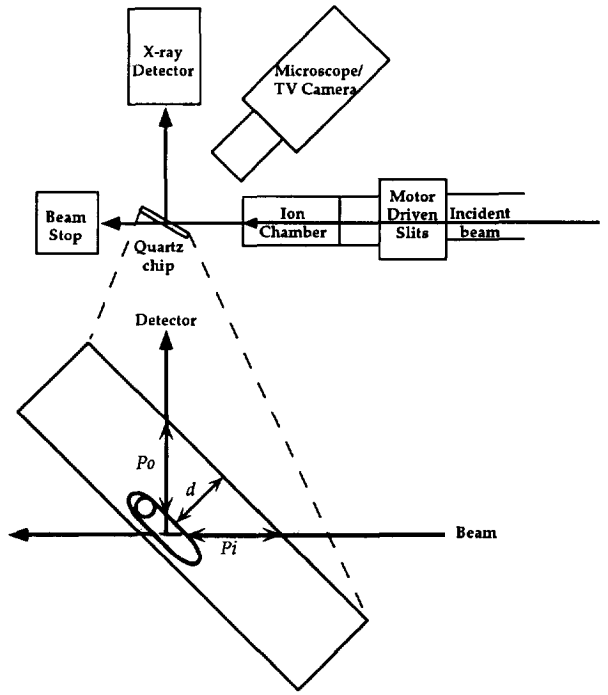

FIG. 1. Schematic diagram of the experimental setup at beamline X26A (from Bassett and Brown, 1990), Inset; schematic diagram of an idealized fluid inclusion in a doubly polished quartz chip. Note the pathlength through quartz of the incoming beam (Pi), and the outgoing X-rays (Po), and the inclusion depth (d). The pathlength of the beam within the inclusion is stippled.

Because light refracts as it enters quartz while the synchrotron X-ray beam does not, the beam location is not always obvious when focusing below the polished surface. Therefore, it is necessary to scan across each inclusion before selecting the spot for analysis. The sample must be carefully examined to insure that there are no other inclusions in the beam path above or below the inclusion of interest. Fig. 2B shows a scan across a fluid inclusion (represented by Fig. 2A) containing 2,662 ppm Sr. The inclusion of interest was analyzed at the point of maximum intensity to insure that the thickest portion of the inclusion was analyzed. SXRF-EDS spectra were collected (for 60–300 seconds), and elemental peaks were identified at characteristic energies.

Two different approaches have been employed to account for the important influence of inclusion geometry on quantitative SXRF analysis. Vanko et al. (1993) select for analysis only inclusions which are smaller than the beam, so that the beam encounters the entire inclusion as it traverses the sample—this approach obviously is well-suited for multiphase inclusions containing several daughter minerals. In the present study only two-phase, liquid-vapor inclusions which were considerably larger than the beam were analyzed. With the former technique, one need only determine the volume of the entire inclusion, and this may be accomplished relatively accurately using a variety of techniques (cf. Bodnar, 1983; Anderson and Bodnar, 1993). With the latter approach, the analytical volume is approximated by a rectangular prism, and the location and size of that prism within the inclusion must be known. In this study each inclusion analyzed was viewed from the side (rotated 90° from the polished surface) in the spindle stage and its maximum thickness was

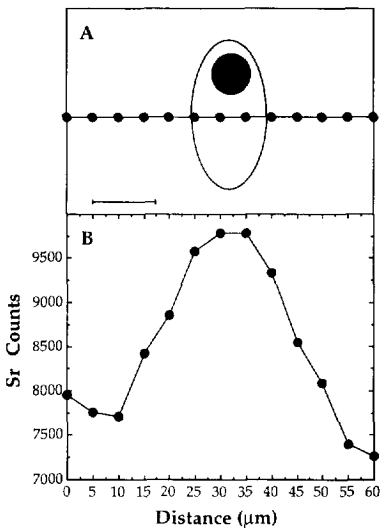

FIG. 2. Sr X-ray counts vs. distance for a scan across a fluid inclusion containing 2662 ± 639 ppm Sr. The scale bar represents the approximate beam width in the scan direction (12 μm).

measured. Each inclusion was analyzed with the incoming beam centered on this thickest part of the inclusion. By multiplying the pathlength through the inclusion by the beam dimensions (8 × 12 μm) the analytical volume within that inclusion was determined. As the beam pierces through a single inclusion, the analytical volume is approximated by a parallelepiped with dimensions of 8 μm × 12 μm × inclusion thickness, and with the top and bottom of the fluid inclusion forming its ends. For each inclusion analyzed, a spectrum was also collected from the quartz host next to the inclusion to determine background concentrations of the metal(s) of interest. In synthetic fluid inclusion samples, background elements are essentially nil, but in natural samples the quartz can contribute significant counts, making it difficult to determine when the beam is on the inclusion, and complicating the quantification process.

One of the major difficulties associated with quantitative SXRF analysis of fluid inclusions concerns estimation of self-absorption corrections to account for low-energy X-rays that are generated within the inclusion but are absorbed by the inclusion fluid. To address this problem, capillaries containing solutions similar to those in the inclusions were analyzed as reference standards, thereby eliminating the need for self-absorption corrections. This approach assumes that the amount of self absorption by solutions in capillaries is similar to that which occurs within inclusions containing the same elements and with the same analytical volume.

After all of the spectra were collected, background-subtracted peak areas were obtained via standard peak-fitting routines. As with electron microprobe analyses, standard measurements were collected immediately before and/or after each analysis to minimize the uncertainties related to variable beam current during analysis. At the NSLS, electrons are injected into the synchrotron ring approximately every 18–24 hours. Immediately following injection, the beam current is at a maximum but decreases continuously until the next injection cycle. As the beam current decreases following injection, peak intensities for a given inclusion (or capillary) also decrease. We correct for this time-intensity effect by using the ion chamber current (the beam current measured just upstream of the sample, Fig. 1) as a proportionality factor to correct and compare spectra taken at different times, i.e., different beam intensities.

Measured intensities were corrected for absorption of both the incoming X-ray beam and the outgoing X-rays generated by the sample as they pass through the same thickness of quartz. Correction factors as a function of inclusion depth in quartz, inclusion thickness, and concentration were calculated for Sr, Fe, Mn, Zn, Pb, and Cu using the Naval Research Lab XRF correction program (NRLXRF) (Criss, 1977). Although the present study is concerned only with Sr, the

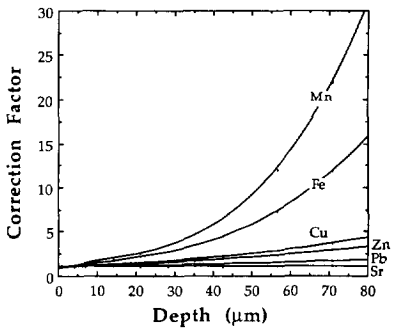

FIG. 3. Plot of correction factor vs. depth in quartz (μm) for Mn, Fe, Cu, Zn, Pb, and Sr.

correction factors of these additional elements were determined for use in a parallel investigation of metals in fluid inclusions from porphyry copper deposits (Bodnar et al., 1993). NRLXRF predicts the counts produced by a given composition and density, as well as the absorption of the incoming and outgoing beams by quartz. The ratio of these two predictions (the counts produced by a specific element in the analytical volume assuming there was no quartz filtering the X-rays, divided by the counts for that element after passing through a given thickness of quartz) yields the factor (CF) that must be multiplied by the counts obtained from a fluid inclusion of given depth to compensate for the absorption effects of the quartz host. For inclusion thicknesses of 1–30 μm and concentrations from 500–50,000 ppm, the correction factors are essentially independent of concentration and inclusion thickness, depending only on the thickness of quartz traversed by the incoming beam and the generated X-rays. Correction factors are presented graphically in Fig. 3 as a function of depth in quartz. For any inclusion in quartz whose depth is known, the correction factor is calculated using the equations in Table 1.

SXRF analyses of standard solutions in silica-glass capillaries of known inner and outer diameter were used to demonstrate the correlation between measured counts and analytical volume—the volume of solution encountered by the beam. Scans of empty capillaries detected only silica. Five-centimeter long, open-ended capillaries of three different sizes (11, 32, and 50 μm i.d., 140 μm o.d.) were suspended vertically into a single solution reservoir guaranteeing that each capillary contained the same solution and assuring that each capillary was full of solution. Thus, analyses from three different analytical volumes were obtained for each concentration. Scans across capillaries containing any of the elements considered in this study (Mn, Fe, Cu, Zn, Pb, and Sr) produce bell-shaped curves, with maximum counts produced at the point where the beam traverses through the center of the capillary. At this point, the analytical volume within the capillary (for an 11 μm i.d. capillary and an 8 × 12 μm beam: the analytical volume is a cylinder of radius 5.5 μm, 8 μm in height, $\pi r^2 h = 760\ \mu m^3$) and the thickness of glass encountered by the beam are known. Figure 4 shows the results of horizontal scans across three capillaries of different volume, all containing 1 wt% Sr.

One concern with the experimental design described above was that some water may have evaporated through the upper open end of the capillary during analysis, particularly if there was any significant heating of the solution by the X-ray beam. To test this, analyses were conducted at various positions along the vertical length of several capillaries. The results showed no variation in elemental counts as a

Table 1. Correction factors (CF) as a function of depth (d, μm) in quartz for Mn, Fe, Cu, Zn, Pb, and Sr.

Mn	CF = 8.5835e-1 + 9.5860e-2(d) - 2.1535e-3(d^2) + 7.0717e-5(d^3)
Fe	CF = 9.6157e-1 + 5.0650e-2(d) - 3.2191e-4(d^2) + 2.5059e-5(d^3)
Cu	CF = 9.9480e-1 + 1.9730e-2(d) + 1.1483e-4(d^2) + 2.0200e-6(d^3)
Zn	CF = 1.0000 + 1.5446e-2(d) + 8.9865e-5(d^2) + 9.9728e-7(d^3)
Pb	CF = 1.0006 + 7.2692e-3(d) + 3.5925e-5(d^2) + 1.3443e-8(d^3)
Sr	CF = 1.0001 + 3.3786e-3(d) + 6.4579e-6(d^2) - 2.0098e-9(d^3)

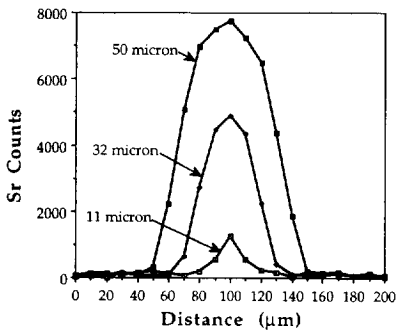

FIG. 4. Strontium intensity vs. distance (μm) for scans across capillaries of 11, 32, and 50 μm inner diameter containing 1 wt% Sr. Step size equals 10 μm.

function of position along the capillary. If evaporation was occurring, we would expect higher counts (higher metal content) at the top of the capillary near the solution-air interface where water loss from the solution would be occurring—this was not observed.

Spectra for sets of capillaries containing three different solutions were collected at the point along the horizontal scan of each capillary where the counts were at their maximum (Fig. 4). Counts were corrected for absorption by the capillary walls using the program NRLXRF (Criss, 1977). The analytical volume within the capillary plotted against the measured (corrected) Sr counts shows a linear relationship for each composition (Fig. 5). The measured counts from any aqueous solution depend (at least in part) upon the volume of that solution encountered by the beam. Therefore, it is clear that to accurately measure metal concentrations in fluid inclusions the analytical volume within each inclusion must be accurately known. The concentration of a metal in an unknown solution is defined by

$$\frac{(CC^{\text{stand.}})/(IC^{\text{stand.}})}{(C^{\text{stand.}})(V^{\text{stand.}})} = \frac{(CC^{\text{sample}})/(IC^{\text{sample}})}{(C^{\text{sample}})(V^{\text{sample}})}, \quad (1)$$

where CC = corrected counts, IC = ion chamber current, V = volume, and C = concentration. Superscripts stand. and sample refer to the capillary standard and fluid inclusion, respectively.

Solving for C^{sample},

$$C^{\text{sample}} = \frac{(C^{\text{stand.}})(V^{\text{stand.}})(IC^{\text{stand.}})(CC^{\text{sample}})}{(CC^{\text{stand.}})(IC^{\text{sample}})(V^{\text{sample}})}, \quad (2)$$

provides the concentration of the element of interest in a specific fluid inclusion.

To test the validity of using solutions in capillaries as standards, and to test if SXRF analyses of solutions of known analytical volume produce accurate results, we used capillary analytical results to calculate concentrations of solutes in other capillaries in the same set (all containing the same solution). Two sets of capillaries containing 1,000 ppm Zn were analyzed by SXRF. The counts and volumes were used as standards to calculate the Zn concentrations in the other five capillaries. The calculated concentrations ranged from 801–1,240 ppm (801, 840, 1048, 1190, and 1,240), with a mean of 1024 ppm Zn. In the same manner, two sets of capillaries containing 10,000 ppm Sr produced Sr concentrations ranging from 8,994–11,126 ppm Sr (8994, 9267, 9,527, 10,420, and 11,126), with a mean of 9,867 ppm Sr. These analyses suggest that our analytical technique provides estimates of Zn and Sr concentrations in capillaries of known dimension with an error of ±20%. If we assume that capillaries represent ideal fluid inclusions, this error then represents the best accuracy one should expect from inclusion analyses.

3. SYNTHETIC FLUID INCLUSION STANDARDS

To test the applicability of the SXRF analytical technique described for capillaries to fluid inclusions, inclusions of known metal content were required. In the early stages of this project, inclusions containing Fe, Cu, Zn, and Ag were synthesized because these metals are of interest in studies of many ore-forming systems. SXRF spectra obtained from inclusions from these early experiments lacked peaks for some of the elements that were dissolved in the solutions that were loaded into the Pt capsules. Therefore, it appeared that the inclusions did not trap solutions of the same composition as that loaded into the capsule. When the fluids remaining in each capsule after each run were analyzed by AAS, metal concentrations were always lower than the starting composition. Therefore, during the hydrothermal run the composition of the solution changed, and the inclusions formed during the run trapped solutions of a lower concentration than the starting composition, yet higher than the final composition in the capsule at the end of the run. The discrepancy between the starting composition and that trapped in the inclusions was assumed to be due to one or both of the following processes: (1) alloying of the metal with the Pt capsule (for Sn and Cu, see Keppler and Wyllie, 1991) and (2) metal silicate formation.

To test our analytical technique, a metal that did not alloy with Pt nor readily form silicates was required. It was also desirable to have a metal whose concentration in individual inclusions could be determined by an independent technique for comparison with the SXRF analyses. Strontium meets both of these criteria and was selected to test our analytical technique. The freezing-point depression of $SrCl_2$ solutions is known (Weast, 1976), allowing the Sr concentration in individual inclusions to be confirmed by microthermometry. Furthermore, Sr silicates are uncommon, thereby minimizing the possibility of Sr silicate formation. Finally, the energetic Sr X-rays are not significantly attenuated by quartz (Fig. 3), thereby minimizing errors resulting from the necessary corrections involved in SXRF analyses.

Strontium chloride solutions of various concentrations were loaded into Pt capsules for fluid inclusion synthesis and the fluid remaining in the capsule after completion of the hydrothermal run was analyzed by atomic absorption. As with the metals Fe, Cu, Ag, and Zn described above, we found that the final Sr concentration of the solution in the capsule at the end

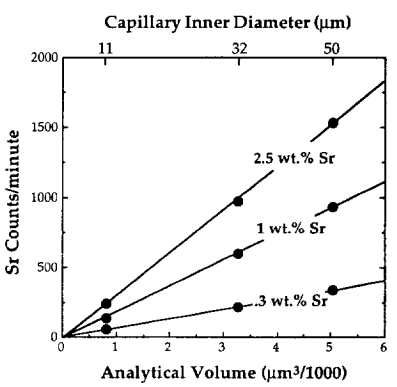

FIG. 5. Sr intensities vs. analytical volume for capillaries containing 0.3, 1, and 2.5 wt% Sr. X axis represents capillary inner diameter (upper axis) and calculated analytical volume (lower axis). Each measurement was collected at the position of maximum intensity of a scan across each capillary as shown in Fig. 3.

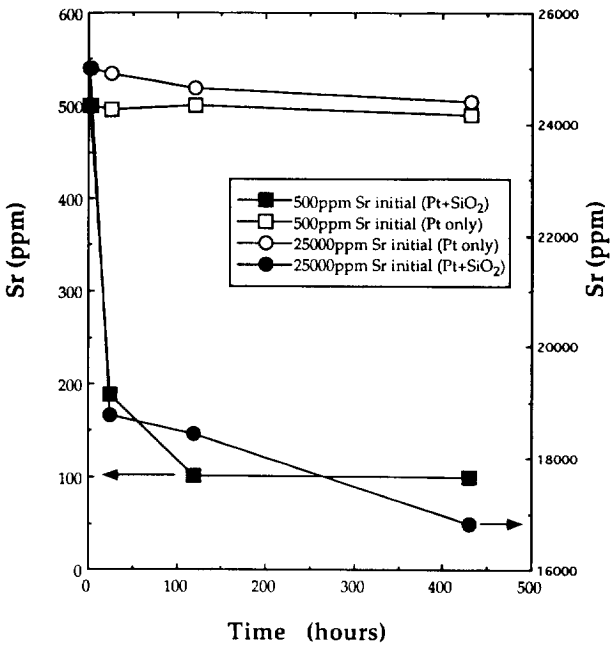

FIG. 6. Strontium concentration vs. time in $SrCl_2$-H_2O solutions during hydrothermal experiments in sealed platinum capsules. Starting solutions contained 25,000 ppm Sr (square symbols-scale on right axis) and 500 ppm Sr (circular symbols-scale on left axis), solid symbols represent runs containing quartz, open symbols represent solution only.

of the synthesis run was lower than the starting concentration. The observation that the Sr concentration after the run was always lower than that initially loaded into the capsule was troubling. In an effort to understand why (and where) Sr was being lost during fluid inclusion synthesis, a simple experiment was performed. Two sets of Pt capsules of equal size were loaded with 150 μl of $SrCl_2$ solutions of different Sr concentrations (500 and 25,000 ppm Sr). One set contained only those solutions, while the other set contained solution plus 0.08 grams of fine-grained quartz. The capsules were sealed, placed in cold-seal bombs and held at 600°C and 2,000 bars for 24, 120, and 430 hours. Upon quenching, solutions were removed from the capsules and analyzed by AAS for Sr. The results (Fig. 6) show no Sr loss in experiments without quartz, but significant Sr loss in the capsules containing quartz. Most of the Sr loss occurred during the shortest (24 hour) experiment with little additional loss observed in the two longer duration experiments (Fig. 6). Therefore, we assumed that the mechanism for Sr loss from solution involved interaction of the Sr in solution with quartz, either by the formation of Sr ($\pm$Cl) silicates during the run or by adsorption of Sr^{++} onto quartz surfaces. SEM analyses of the solid material (quartz) removed from the Pt capsules at the completion of the experiments detected no Sr, nor did XRD analyses detect the presence of Sr or Sr-chloro-silicates. Therefore, we assume that Sr loss from the solutions during the hydrothermal runs was the result of adsorption of Sr onto quartz surfaces, in concentrations below the detection limits of XRD and SEM analyses. Similar problems with adsorption of highly charged (+2, +3) cations onto quartz during crush-leaching analysis was observed by Bottrell et al. (1988). Although we do not have a clear understanding of the mechanism(s) responsible for Sr loss from solution, the results of the present study are not affected by this problem because we are able to determine the Sr concentration in each of the inclusions analyzed by SXRF from freezing-point depression measurements.

Final-melting temperatures for all inclusions were measured to determine the $SrCl_2$ content of each inclusion before SXRF analyses were attempted. All inclusions in a single fracture yielded the same melting and homogenization temperatures ($n > 12$ per fracture) thereby ruling out Sr variability within a single population. The initial and final concentrations were combined with the concentrations determined by heating/freezing measurements to determine the possible range of Sr concentrations present in each sample. For example, freezing-point determinations bracket the concentration of inclusions in sample 100593-III between 3,594 and 5,441 ppm Sr, yet the upper limit was set by the initial composition of 5,000 ppm Sr (Table 2) resulting in a combined range of 3,594–5,000 ppm Sr, or 4,340 $\pm$ 660. The concentration and uncertainties for each sample were established in a similar manner and are presented in Table 2. Thus, seven sets of samples of known Sr concentration were available for quantitative SXRF analysis.

Note that the freezing points of fluid inclusions can only be measured to $\pm$0.05°C. This temperature range corresponds to a range in Sr concentration of about 1800 ppm. Thus, the reported concentration of 5,441 ppm Sr corresponds to a freezing-point depression of -0.3°C, but the actual freezing-point depression could be between 0.25 and 0.35°C, corresponding to Sr concentrations of 4442 and 6200 ppm, respectively. It is inconceivable that the Sr concentration in the inclusion could be higher than that originally loaded into the capsule. Thus, when the freezing-point depression indicates a

Table 2. Analytical results obtained from $SrCl_2$-bearing synthetic fluid inclusion standards.

Sample Number	Starting Composition (ppm)	Final Composition (ppm)	Melting Temp (°C)	Melting T Composition (ppm)	Composition (ppm)
92293-V	500	247	0> X>-.1	0 - 1723	374 +/- 126
92293-VI	1000	569	0> X>-.1	0 - 1723	785 +/- 216
22294-I	3000	*	-.1> X>-.2	1723 - 3594	2362 +/- 639
100593-III	5000	3680	-.2> X>-.3	3594 - 5441	4340 +/- 660
92293-VIII	10000	*	-.5> X>-.6	9069 - 10850	9535 +/- 466
22294-III	25000	15100	-.9> X>-1.1	16050 - 19410	17730 +/- 1680
50693-III	35000	22040	-1.3> X>-1.5	22670 - 25850	24260 +/- 1590

* Not enough fluid for reliable measurement

Sr concentration higher than the initial value as a result of the relatively poor sensitivity of the freezing-point depression measurement, as in the above example, the concentration originally loaded into the capsule is taken as the upper limit.

4. RESULTS

Using Eqn. 2 and results from SXRF spectra and inclusion analytical volume determinations, Sr concentrations were calculated for inclusions in five of the seven samples examined in this study. Fluid inclusions in samples containing 374 (±126) and 785 (±216) ppm Sr did not yield adequate Sr counts for analysis. Twenty seconds/point scans across these inclusions did not yield significant Sr counts above background, even for inclusions as shallow as 14 μm.

The detection limit for metals in fluid inclusions as determined by SXRF is a function of host sample thickness, inclusion thickness, metal concentration in the inclusion, background metal concentration in the host quartz, and inclusion depth. Because the detection limit is also a function of the excitation energy spectrum, elements with X-ray energies closer to the incoming maximum, such as Fe or Zn, have lower detection limits than Sr. In 11 μm inner diameter capillaries, the detection limit for Sr is approximately 250 ppm. However, in quartz the greater total sample thickness, and especially the abundant trace elements present in the host, increase the background tenfold over that from silica glass capillaries. Ideally, quartz chips containing fluid inclusions could be thinned to minimize the background. Unfortunately, thin quartz chips tend to break when manipulated in oil in the spindle stage to determine inclusion depths and geometries. An alternative approach would be to thin the quartz chips after completion of the spindle stage measurements (and before SXRF analyses), but thickness measurements must be rechecked after SXRF analyses at the exact position and orientation of the beam in the sample. Although we preselect inclusions for analysis before taking the sample to the beam line, it is not possible to predetermine with any degree of accuracy the orientation of the sample (and the inclusion) in the X-ray beam. Thus, although we measure geometries and path lengths of inclusions to be analyzed before the analysis is conducted, these measurements must be verified and sometimes modified by repeating the spindle stage measurements after the SXRF analyses are completed.

Inclusions in seven samples were analyzed using SXRF. However, none of the inclusions in samples containing 374 (±126) and 785 (±216) ppm Sr, even those inclusions within 5 μm of the upper surface, provided spectra that could be quantified. Scans across inclusions containing 2,362 (±639) ppm Sr that were less than 4 μm thick, and within 12 μm of the upper surface, yielded no Sr peak above background. For thicker inclusions, Sr could be detected and quantified in inclusions containing 2,362 ppm Sr—thus, the Sr detection limit is lower than 2,362 ppm, but greater than 785 ppm because inclusions containing 785 (±216) ppm Sr were below detection. The detection limit for Sr in fluid inclusions is, therefore, between 785 and 2362 ppm Sr. In this study, inclusion thickness ranged from 4–18 μm (with the exception of one 30 μm thick inclusion). Strontium can be measured reliably in inclusions as deep as 300 μm (in quartz) but analysis of lighter elements is only possible for much shallower fluid inclusions (see Vanko et al., 1993).

The results of analyses of thirty three individual inclusions from samples containing five different Sr concentrations are presented in Table 3. The known concentration range for each sample is listed above the inclusion numbers. Also shown are depth, correction factor (C.F.), corrected counts, inclusion thickness, and the calculated Sr concentration (ppm). The mean for each sample and the standard deviation are also listed. Most individual inclusion analyses did not fall within the known concentration range for that sample (defined by combining the starting and ending fluid compositions of each run with the compositions obtained from the freezing-point depression measurements of each inclusion in the sample), but the mean concentration of all of the inclusions in a sample was within the known concentration range for three samples containing 2,362 (±639) ppm, 9,535 (±466) ppm, and 24,260 (±1590) ppm. The mean of the analyses of the other two samples, containing 4,340 (±660) ppm and 17,730 (±1,680) ppm, fell within one standard deviation of the known concentration range.

The known concentrations (Table 3) are plotted against concentrations determined from SXRF analyses (Table 3) in Fig. 7, illustrating both the large range in individual inclusion results as well as the close proximity of the mean measured concentrations to the known concentrations (solid diagonal line). Note that the known composition of any single inclusion lies somewhere within the horizontal error bars for that sample, which represents the uncertainty in the known concentration. If that horizontal uncertainty is applied over the entire range of the standard deviation of the measured concentrations, represented by the vertical error bars, then the known composition of all of the samples falls within one standard deviation (1σ) of the measured compositions. Although the magnitude of the variance (in ppm) increases with increasing concentration, when examined as a percentage of the mean, standard deviations (1σ) vary from 10–39% of the mean with no correlation between concentration and the degree of scatter.

5. DISCUSSION

The goal of this study was to determine the reliability with which quantitative analyses of individual fluid inclusions could be obtained with SXRF and to identify those analytical factors which most affect quantitative analyses. The major uncertainty in these analyses is the determination of the analytical volume within fluid inclusions. As the capillary analyses showed, an incorrect analytical volume estimate can affect the calculated concentration. For a 2.5 wt% Sr solution in silica-glass capillaries (Fig. 5) an order of magnitude change in the analytical volume (from 500–5,000 μm^3) produces an order of magnitude change in the Sr counts (from 160–1,600 counts/minute). Therefore, an order of magnitude error in the inclusion thickness measurement would produce an order of magnitude increase in the calculated concentration. A. J. Anderson and R. J. Bodnar (unpub. data) compared fluid inclusion volumes calculated from spindle stage measurements with those calculated by the method of Bodnar (1983). During that investigation, they found that the error

Table 3. Analytical results obtained from 33 individual fluid inclusions of five different $SrCl_2$ concentrations. Fluid inclusion Sr-concentrations (bold case) and sample numbers (italics) are listed for each sample.

Fluid Inclusion#	Depth (μm)	C.F.	Corr. counts	Thick (μm)	Sr ppm	Mean	Stand. Dev.
2362 +/- 639 ppm							
22294-I-							
2	90	1.36	5247.71	9	2457.69	2661.8	280.70
3	100	1.40	6252.79	10	2648.95		
5	160	1.72	3733.80	7	2477.92		
16	60	1.23	6709.14	10	3062.72		
4340 +/- 660 ppm							
100593-III-							
5	60	1.23	3978.87	4	2440.94	2802.9	690.2
6	52	1.19	5022.40	8	3002.57		
7	190	1.90	6183.35	7.5	2023.11		
11	72	1.28	3324.50	8	2189.36		
13	70	1.27	5134.37	7	3491.28		
14	100	1.40	7708.59	10	3670.59		
9535 +/- 466 ppm							
92293-VIII-							
1	5	1.02	3469.88	18	10538.24	9244.5	1313.6
2	37	1.13	1384.60	9	8434.04		
3	30	1.11	1420.76	10	7824.76		
4	27	1.10	1466.22	10	7745.58		
8	85	1.33	1571.73	10	8978.21		
9	95	1.38	2029.80	11	10736.37		
10	59	1.22	2178.65	12	10454.15		
17730 +/- 1680 ppm							
22294-III-							
1-1	5	1.02	10231.02	7	12528.15	14684.3	3469.7
1-2	22	1.08	5898.61	4	12683.54		
1-3	31	1.11	12799.42	9	12221.57		
2-4	120	1.50	20243.05	10	16890.52		
2-5	100	1.40	29806.73	14	17431.52		
2-9	90	1.36	5805.45	4	12130.12		
2-10	55	1.21	10128.23	6	14084.75		
2-12	85	1.33	5810.58	4	12060.57		
2-13	55	1.21	48013.87	18	22128.07		
24,260 +/- 1590 ppm							
50693-III-							
1	21	1.07	67165.15	15	28187.20	22588.9	8785.1
2	16	1.06	15540.22	13	16683.14		
3	46	1.17	42467.59	15	19440.70		
5	25	1.09	46940.99	12	24583.15		
6	70	1.27	11273.04	8	10143.07		
12	5	1.02	180996.95	30	37646.83		
15	27	1.10	10705.69	7	21437.86		

Depth (μm) = Distance from upper quartz surface to the top of the fluid inclusion.
C.F. = Correction factor (see Fig. 3).
Corr. Counts = Sr counts obtained from the inclusion after correction (counts * C.F.).
Thickness (μm) = The pathlength traversed by the beam through the fluid inclusion.
Sr (ppm) = Sr concentration in the fluid inclusion calculated from SXRF measurements.
Mean = The mean of all analyses from a single sample.
Stand. Dev. = The standard deviation of all analyses from a single sample.

in the inclusion thickness measurement using the spindle stage is approximately ±0.3 μm. Assuming an error of this magnitude in our measurements, a fluid inclusion 10 μm thick would yield an analytical volume (with an 8 × 12 μm beam) of 960 μm^3 ± 28 μm^3 (3% error), while a fluid inclusion 3 μm thick would yield an analytical volume of 288 μm^3 ± 68 μm^3 (23% error). Thus, the minimum error of the volume estimates presented herein is in the range 3–23%.

The path lengths through fluid inclusions that are highly irregular in three dimensions are difficult to determine accurately with the spindle stage. Fluid inclusions of constant thickness that lie parallel to the upper polished surface yield the most consistent SXRF quantitative results because the path length through these inclusions (and, therefore, analytical volume) can be determined more accurately. In samples that contain numerous inclusions at different orientations relative to the beam, path lengths through these inclusions are some unknown value greater than the apparent inclusion thickness. Thus, these inclusions yield highly variable calculated concentrations because of inaccurate analytical volume

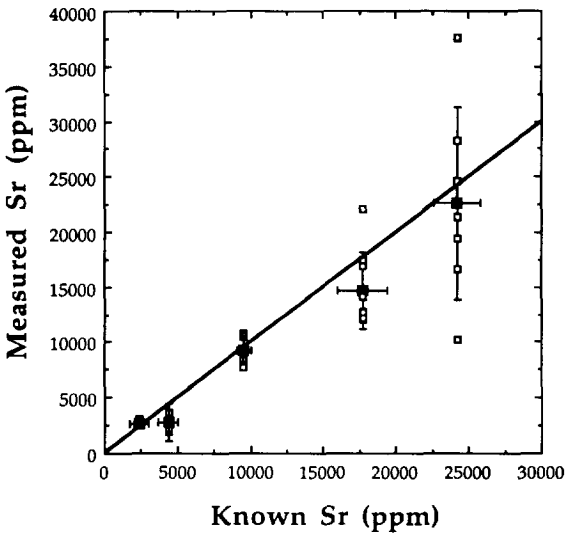

FIG. 7. Plot of measured Sr vs. known Sr for thirty three individual fluid inclusions (open boxes) from samples of five different Sr concentrations. Solid squares represent the mean of the measured values for each sample, error bars in the y direction represent the standard deviation for that sample, the error bars in the x direction represent the uncertainty of the known Sr concentration for each sample. The dark black line has a slope of 1 for comparison.

determinations, thereby adding yet another uncertainty to the overall analysis.

The large uncertainty associated with individual fluid inclusion analyses, combined with the very good correlation between the mean (of numerous analyses within a population) and the known concentration, demands that numerous inclusions within one population be measured and averaged if a representative metal concentration for that population is to be obtained. Furthermore, flat-lying, equant, regularly-shaped inclusions should be chosen for analysis if quantitative results are sought. In all cases, one should select large inclusions, as close to the upper polished surface of very clear quartz as possible. We have found that, as a rule thumb, if an inclusion is close enough to the surface to be seen clearly during reflected-light petrographic examination, it is probably sufficiently close to the surface to obtain an SXRF spectrum for many metals.

As with all fluid inclusion studies, fluid inclusion populations should be identified based on paragenetic studies of crosscutting inclusion trails, petrographic observations, and heating/freezing results (Bodnar, 1994), and not from SXRF analyses. Unfortunately, the current poor precision of SXRF analyses precludes the use of this analytical technique to monitor minor variability in metal concentrations within a fluid inclusion population.

Given the severe limitations of other fluid inclusion analysis techniques (correction problems, fluid inclusion generation mixing, inclusion decrepitation, etc.) SXRF may provide the only truly nondestructive analytical technique for the analysis of individual fluid inclusions. Because of its extremely reliable spatial resolution, SXRF is particularly useful for identifying daughter phases within fluid inclusions. In deposits containing highly concentrated solutes (such as rare element pegmatites or porphyry Cu systems) the identification of daughter phases can provide important insights into the nature of hydrothermal fluids attending mineralization.

The concentrations of Sr in inclusions examined in this study are much higher than would be expected in most natural inclusions. However, the purpose of this study was to characterize those features which most influence quantitative analysis with SXRF, and not to simulate natural inclusion metal compositions or concentrations. During reconnaissance investigations of fluid inclusions from rare element pegmatites, we have detected Sr daughter minerals, resulting in calculated Sr concentrations of >50,000 ppm. The relatively high detection limits reported herein preclude meaningful analyses of fluid inclusions from most nonmagmatic ore deposits. Our preliminary investigations of fluid inclusions from a variety of sediment-hosted ore deposits, including several Mississippi Valley-type deposits, have been unsuccessful because these inclusions apparently contain low concentrations of metals. Furthermore, the high levels of trace elements in natural samples, and the presence of abundant solid inclusions of variable composition intimately associated with fluid inclusions in these samples, makes their quantification difficult at best.

Acknowledgments—We are greatly indebted to Sarah Beutner Mavrogenes for the extensive sample preparation necessary for this study. Dave Vanko, Mo Ghazi, Andy Campbell, and an anonymous reviewer are thanked for thoughtful reviews of an earlier version of this manuscript. Funding for this work was provided by National Science Foundation grants EAR 9316051 and EAR 9305032 to RJB.

Editorial handling: D. A. Vanko

REFERENCES

Anderson A. J. and Bodnar R. J. (1993) An adaptation of the spindle stage for geometric analysis of fluid inclusions. *Amer. Mineral.* **78,** 657–664.

Anderson A. J., Clark A. H., Ma Xin-Pei, Palmer G. R., and MacArthur J. D. (1989) Proton-induced X-ray emission analysis of unopened fluid inclusions. *Econ. Geol.* **84,** 924–939.

Barnes H. L. (1979) Solubilities of ore minerals. In *Geochemistry of Hydrothermal Ore Deposits*, 2nd ed. (ed. H. L. Barnes), pp. 404–460. Wiley.

Bassett W. A. and Brown G. E., Jr. (1990) Synchrotron radiation: Applications in the earth sciences. *Ann. Rev. Earth Planet. Sci.* **18,** 387–447.

Bodnar R. J. (1983) A method of calculating fluid inclusion volumes based on vapor bubble diameters and *p-v-t-x* properties of inclusion fluids. *Econ. Geol.* **78,** 535–542.

Bodnar R. J. (1994) Philosophy of fluid inclusion analysis. In *Fluid Inclusions in Minerals, Methods, and Applications* (ed. B. De Vivo and M. L. Frezzotti), p. 1–6, Virginia Polytech. Inst. State Univ.

Bodnar R. J., Mavrogenes J. A., Anderson A. J., Bajt S., Rivers M. L., and Sutton S. (1993) Synchrotron XRF evidence for the sources and distributions of metals in porphyry copper deposits. *Amer. Geophys. Union Trans. EOS* **74,** 669.

Bottrell S. H., Yardley B., and Buckley F. (1988) A modified crush-leach method for the analysis of fluid inclusion electrolytes. *Bull. Mineral.* **111,** 279–290.

Carpenter A. B., Trout M. L., and Pickett E. E. (1974) Preliminary report on the origin and chemical evolution of lead- and zinc-rich oil field brines in central Mississippi. *Econ. Geol.* **69,** 1191–1206.

Criss J. (1977) NRLXRF, Naval Research Laboratory Cosmic Program #DOD-00065. Naval Research Laboratory, Washington, D.C.

Frantz J. D., Mao H. K., Zhang Y.-G., Wu Y., Thompson A. C., Underwood J. H., Giauque R. D., Jones K. W., and Rivers M. L.

(1988) Analysis of fluid inclusions by X-ray fluorescence using synchrotron radiation. *Chem. Geol.* **69,** 235–244.

Haynes F. M., Sterner S. M., and Bodnar R. J. (1988) Synthetic fluid inclusions in natural quartz IV. Chemical analyses of fluid inclusions by SEM/EDA: Evaluation of method. *Geochim. Cosmochim. Acta* **52,** 969–977.

Heinrich C. A., Ryan C. G., Mernaugh T. P., and Eadington P. J. (1992) Segregation of ore metals between magmatic brine and vapor: A fluid inclusion study using PIXE microanalysis. *Econ. Geol.* **87,** 1566–1583.

Helgeson H. C. (1992) Effects of complex formation in flowing fluids on the hydrothermal solubilities of minerals as a function of fluid pressure and temperature in the critical and supercritical regions of the system H_2O. *Geochim. Cosmochim. Acta* **56,** 3191–3207.

Horn E. E. and Traxel K. (1987) Investigations of individual fluid inclusions with the Heidelberg proton microprobe-a nondestructive analytical method. *Chem. Geol.* **61,** 29–35.

Keppler H. and Wyllie P. J. (1991) Partitioning of Cu, Sn, Mo, W, U, and Th between melt and aqueous fluid in the system haplogranite-H_2O-HF. *Contrib. Mineral Petrol.* **109,** 139–150.

Maaskant P. (1986) Electron probe microanalysis of unopened fluid inclusions, a semiquantitative approach. *Neues Jahrb. Mineralogie Monatsch.* **7,** 297–304.

Rankin A. H., Ramsey M. H., Coles B., Van Langevelde F., and Thomas C. R. (1992) The composition of hypersaline, iron-rich granitic fluids based on laser-ICP and synchrotron-XRF microprobe analysis of individual fluid inclusions in topaz, Mole granite, eastern Australia. *Geochim. Cosmochim. Acta* **56,** 67–79.

Rivers M. L., Sutton S. R., and Jones K. W. (1991) Synchrotron X-ray fluorescence microscopy. *Synchr. Rad. News* **4,** 23–26.

Roedder E. (1990) Fluid inclusion analysis: Prologue and epilogue. *Geochim. Cosmochim. Acta* **54,** 495–507.

Shepherd T. J., Rankin A. H., and Alderton D. H. M. (1985) *A practical guide to fluid inclusion studies.* Blackie.

Symonds R. B. (1992) Getting the gold from the gas: How recent advances in volcanic gas research have provided new insights on metal transport in magmatic fluids. *Geol. Surv. Japan* **279,** 170–175.

Vanko D. A., Sutton S. R., Rivers M. L., and Bodnar R. J. (1993) Major-element ratios in synthetic fluid inclusions by synchrotron X-ray fluorescence microprobe. *Chem. Geol.* **109,** 125–134.

Weast R. C., ed. (1976) *Handbook of Chemistry and Physics.* CRC Press.

Weissberg B. G., Browne P. R. L., and Seward T. M. (1979) Ore metals in active geothermal systems. In *Geochemistry of Hydrothermal Ore Deposits,* 2nd ed. (ed. H. L. Barnes), pp. 738–780. Wiley.